Detailed study of dissipative quantum dynamics of K_2 attached to helium nanodroplets

Martin Schlesinger, Walter T. Strunz

Institut für Theoretische Physik, Technische Universität Dresden, D-01062 Dresden, Germany

E-mail: Martin.Schlesinger@tu-dresden.de

Abstract. We thoroughly investigate vibrational quantum dynamics of dimers attached to He droplets motivated by recent measurements with K_2 [1]. For those femtosecond pump-probe experiments, crucial observed features are not reproduced by gas phase calculations but agreement is found using a description based on dissipative quantum dynamics, as briefly shown in [2]. Here we present a detailed study of the influence of possible effects induced by the droplet. The helium droplet causes electronic decoherence, shifts of potential surfaces, and relaxation of wave packets in attached dimers. Moreover, a realistic description of (stochastic) desorption of dimers off the droplet needs to be taken into account. Step by step we include and study the importance of these effects in our full quantum calculation. This allows us to reproduce and explain all major experimental findings. We find that desorption is fast and occurs already within $2 - 10$ ps after electronic excitation. A further finding is that slow vibrational motion in the ground state can be considered frictionless.

PACS numbers: 33.15.Mt 03.65.Yz, 82.53.-k, 67.25.dw

1. Introduction

Helium nanodroplet isolation (HENDI) spectroscopy allows to study atoms, molecules and clusters embedded in an ideal cryogenic environment [3]. Ultracold helium droplets (0.38 K) provide a gentle, since weakly disturbing host for embedded species, which can be studied with high resolution spectroscopy [4]. However, spectra of immersed species are slightly broadened and shifted away from their gas phase value due to their interaction with the surrounding He droplet. Inhomogeneous broadening in pure rotational spectra is ascribed to the motion of the purity inside the droplet [5, 6] or to coupling to collective degrees of freedom of the droplet [7]. The overall spectral features, which are unseen in gas phase measurements, have been used to study the weak interaction between dopant and helium droplet [8, 9, 10, 5, 11, 12]. Attached species allow to probe the peculiar properties of the superfluid He droplet itself [13]. Further insight into the interaction and the quantum properties of the droplet is gained from recently obtained time-resolved studies [1, 2, 14, 15].

Helium nanodroplets, typically consisting of several thousand ^{4}He atoms, are ideally suited to study relaxation (cooling) of embedded species [16, 17, 18, 19, 20]. Whether dissipation plays a role depends on the involved energy scales, the coupling strengths, or on typical time scales in the system and "bath" [21, 22]. The group of Miller has studied relaxation of the HF system inside He droplets [23] . They report on ineffective vibrational relaxation due to a mismatch in energy scales. However, rotational relaxation in the immersed HF system is fast and appears as Lorentzian line broadening in the rotational transition spectrum. (see also [7] and references therein).

Alkali metal atoms and molecules are known to reside in bubble-like structures on the surface of He droplets [24, 25, 26]. Attached Rb_2 dimers in the triplet state reveal the presence of vibrational relaxation on the measurement timescale [27, 15]. For Lithium dimers interacting with a He environment, vibrational relaxation has been investigated by means of Monte Carlo calculations [28], including a few He atoms. The corresponding relaxation rates depend on whether the dimer is orientated in-plane or out-of-plane with respect to the He surface [29].

Femtosecond pump-probe techniques are established tools to analyze the ultrafast vibrational motion in molecular systems [30, 31, 32]. A first laser pulse excites a coherent wave packet, which is allowed to freely evolve on the respective energy surface. The WP is probed by a time-delayed pulse. Since the early studies by the Zewail group [33, 34], vibrational wave packets in various diatomic systems have been studied, such as Na_2 [35] or K_2 [36, 37, 38]. When molecules are located in a solid rare-gas matrix [39, 40], a suppression of revival structures in the pump-probe signal indicate a loss of vibrational coherence. Meier et. al. have thoroughly investigated such decoherence in molecular systems placed in a rare-gas environment [41], motivated by seminal experiments in the Zewail group [42]. For experiments at room temperature with a significant thermal occupation of rotational states, unavoidable coupling between internal vibrational and rotational degrees of freedom may lead to sufficient decoherence to suppress (fractional)

revivals [43]. Experiments with Rb_2 dimers on He droplets reveal an ongoing decay of the pump-probe ion yield [14]. The decay has been ascribed to damping and accompanying decoherence of vibrational wave packets [15]. In this work we investigate potassium dimers on He droplets, studied experimentally with the pump-probe technique [1]. A brief account of a theoretical description based on dissipative quantum dynamics was given in [2]. Experimental spectra show significant deviations from corresponding gas phase calculations for the unperturbed dimer.

In this paper, in a phenomenological approach, we investigate in detail how the helium influence may be described effectively. First, we see that the helium environment destroys electronic coherence, which is imprinted by the exciting laser pulse. As possible causes for electronic decoherence, we consider a distribution of shifts of electronic surfaces. Electronic decoherence alone cannot account for the decay of the signal at certain excitation wavelengths. Therefore, in a next step, we include a general damping of vibrational wave packets on each electronic surface. The effective dynamics is described by means of a quantum optical master equation.

Moreover, it is important to take into account the desorption of dimers from the droplet properly. No general rule can be given when attached atoms or molecules leave the droplet. It is known that lighter alkali metal atoms leave the droplet upon electronic excitation [44] or form a bound exciplex [45]. The exciplex tends to desorb off the droplet surface during the formation process or several picosecond thereafter [46]. On the other hand, desorption of Rb atoms may be completely inhibited upon electronical excitation in a certain laser wavelength range [47]. Recent measurements indicate that K_2 molecules desorb several picoseconds after laser excitation [1]. Indeed, (stochastic) desorption of dimers are a crucial ingredient to explain spectral features with a theoretical model [2].

We here report on a more realistic description of desorption - we use a model which only allows electronically excited molecules to leave the droplet. We thus extend our previous, state-independent desorption scheme [2]. Together with dissipation and shifts of potential energy surfaces, one can explain experimental findings over the full laser excitation range reported in [1].

The article is organized as follows: In section 2 we review the calculation of the pump-probe signal for free dimers. In the following section 3, the influence of the helium environment is considered in a phenomenological way. In section 3.3 we explain how we treat desorption of dimers. Finally, for an even better agreement with experiment, we consider undamped motion in the electronic ground state. A thorough comparison between theoretical and experimental findings is given at every step in the model. Section 4 is devoted to the conclusions.

2. Pump-probe signal

A first "pump" laser pulse creates a vibrational wave packet (WP) $|\psi_i\rangle$ in some electronic state $|i\rangle$. The excited WP oscillates in a region between classical inner and outer turning

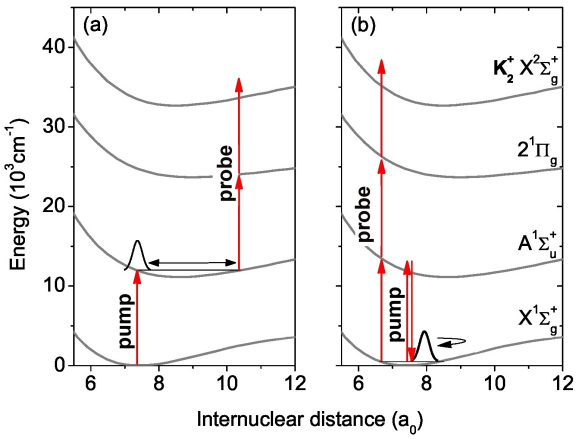

Figure 1. Excitation schemes in the potassium dimer for two distinct laser wavelengths $\lambda = 833\,\mathrm{nm}$ (scheme I) and $\lambda = 800\,\mathrm{nm}$ (scheme II). While the first scheme exclusively maps the WP in the $\mathrm{A}\,^1\Sigma_u^+$ state, the second scheme allows to observe the WP in the ground state $\mathrm{X}\,^1\Sigma_g^+$.

point of that surface. It may periodically enter and leave a transition region, where a resonance condition with higher lying states is met and the potential energy difference matches the second, "probe" pulse energy. This region defines the so-called Franck-Condon (FC) window. The time-delayed probe pulse leads to a significant number of ions only when the WP is located in the FC window. By varying the time delay τ between pump-and probe pulse, one obtains an oscillatory ion yield. A typical excitation scheme is depicted in fig. 1(a), where one probes the dynamics of the WP on the $\mathrm{A}\,^1\Sigma_u^+$ surface.

Wave packets may be excited in several involved electronic surfaces of the dimer. More specifically, the pump pulse prepares the dimer in a superposition of electronic states, such that the full state vector $|\Psi\rangle$ takes the form

$$|\Psi(t_{\mathrm{pump}})\rangle = \sum_i |\psi_i\rangle|i\rangle. \tag{1}$$

Here, ψ_i denotes the WP on a specific electronic state i and

$$p_i = \langle\psi_i|\psi_i\rangle \tag{2}$$

is the probability that the electronic state i is excited.

For the pump-probe signal, we fully numerically solve the time-dependent Schrödinger equation (TDSE)

$$i\hbar\frac{\partial}{\partial t}\begin{pmatrix}\psi_0\\ \psi_1\\ \psi_2\\ \psi_3(E)\end{pmatrix} = \begin{pmatrix}H_0 & J_{01} & 0 & 0\\ J_{10} & H_1 & J_{12} & 0\\ 0 & J_{21} & H_2 & J_{23}^I\\ 0 & 0 & J_{32}^I & H_{3,E}\end{pmatrix}\begin{pmatrix}\psi_0\\ \psi_1\\ \psi_2\\ \psi_3(E)\end{pmatrix}, \tag{3}$$

for the full state vector $|\Psi\rangle$ (see also [48, 36]). In the matrix equation, the diagonal elements denote the molecular Hamiltonian $H_{\mathrm{mol}} = \sum_i H_i = T + \sum_i V_i$, which involves

kinetic energy $T = P^2/2\mu$ (reduced mass μ) and adiabatic potentials V_i. In the final ionic state, the energy E of the ejected electron is included in the diagonal entry of the Hamiltonian $H_{3,E}$, such that $V_{i=final} = V_3+E$. The coupling to the laser field is described by the matrix elements $J_{ij} = -\vec{\mu}_{ij}\cdot\vec{E}(t)$, where $\vec{\mu}_{ij}$ denotes the transition dipole moment. Both pump- and probe pulse have the form $\vec{E}_{\mathrm{pump/probe}}(t) = \vec{\epsilon}_0\varepsilon(t)\cos(\omega_L t)$ and ω_L is the respective laser frequency. Moreover, $\vec{\epsilon}_0$ is the polarization and $\varepsilon(t)$ the shape function of the field, which is assumed to be Gaussian. For the field parameters we use a full width at half maximum of the laser pulse of 110 fs and an intensity of $1.2\,\mathrm{GW/cm^2}$. The employed intensity is higher than the experimentally estimated value (I=$0.5\,\mathrm{GW/cm^2}$ [1]), but, according to [36], still located in the moderate power regime. The ionic state $\psi_3(E)$ also depends on the energy E of the ejected electron. We use discretization of the (electronic) continuum, a technique successfully employed earlier [48]. One determines the final state probability $|\psi_3(E_k)|^2$ after both pulses have passed for distinct electronic energies E_k. The pump-probe signal is proportional to the sum over different electronic contributions,

$$S(\tau) = \lim_{t\to\infty}\sum_{E_k}|\psi_3(\tau, E_k)|^2. \tag{4}$$

In the limit $t \to \infty$ (upon complete decay of the second pulse), it only depends on the delay τ between the pulses. For the propagation of the wave function, we use the split-operator method [49].

The ion signal is composed of beat frequencies $\omega_{vv'} \equiv (E_v - E_{v'})/\hbar$ between all pairs of energy levels that contribute to the WP [15]. The most prominent oscillation originates from the energy spacing between central and neighboring vibrational levels $\bar{v}$ and $\bar{v} \pm 1$. This oscillation has the frequency

$$\omega_i \equiv \omega_{\bar{v},\bar{v}+1} \tag{5}$$

and is characteristic for the electronic surface i. In an anharmonic potential, the level spacing and therefore also ω_i decreases as $\bar{v}$ increases. Higher-order frequency components $\omega_{\bar{v},\bar{v}+\Delta v}$ with $\Delta v > 1$ are visible in the Fourier transform (FT) of the signal.

The laser wavelength λ determines which wave packets ψ_i can be mapped to the final state. In the one-color pump-probe setup, we consider two different excitation schemes.

For $820\,\mathrm{nm} \lesssim \lambda \lesssim 840\,\mathrm{nm}$ (scheme I), one exclusively follows the vibrational dynamics in the excited state $\mathrm{A}\,^1\Sigma_u^+$. The WP in that state can be probed at the outer turning point (see fig. 1(a)). Contributions from other surfaces are negligible. For this scheme we concentrate on an excitation wavelength $\lambda = 833\,\mathrm{nm}$. Fig. 2(a) shows the theoretical gas phase calculation. Fig. 2(b) shows experimental spectra at this wavelength obtained from dimers attached to helium nanodroplets [1]. In the experiment, the signal amplitude significantly decreases, but oscillates with nearly constant amplitude at later delay times.

For $800 \lesssim \lambda \lesssim 820\,\mathrm{nm}$ (scheme II), transitions preferably take place at the inner turning point of the excited WP. The wave packet in the electronic ground state $\mathrm{X}\,^1\Sigma_g^+$

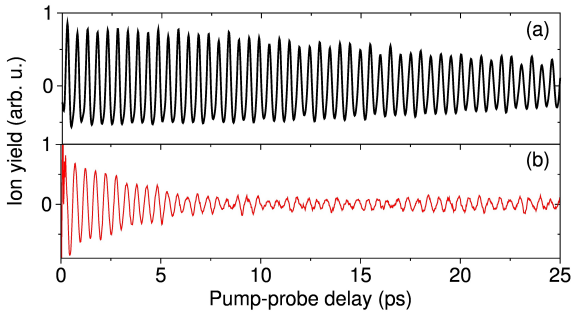

Figure 2. Pump-probe ion yield at $\lambda = 833\,\mathrm{nm}$. (a) Numerical gas phase calculation. (b) Experimental result (from [1]). The oscillation is exclusively attributed to the circulating WP in the $A\,^1\Sigma_u^+$ state.

is excited through resonant impulsive stimulated Raman scattering (RISRS). It can be probed through a 3-photon process, see fig. 1. On the other hand, simultaneous and coherent contributions from WPs in electronic excited states lead to constructive or destructive interferences and thus to an unstructured ion yield [38]. We use sliding window Fourier transforms $\mathcal{F}(\omega, \tau)$ to follow the evolution of respective beat frequency components as a function of the delay time [50, 51]. Fig. 3(a) shows a window transform (spectrogram) for excitation at $\lambda = 800\,\mathrm{nm}$. A frequency component $\omega_A \approx 63\,\mathrm{cm}^{-1}$ can be ascribed to the WP in the state $A\,^1\Sigma_u^+$. Moreover, a higher-order frequency component around $\approx 2\omega_A$ is visible as is a significant contribution at $\omega \approx 85\,\mathrm{cm}^{-1}$ after about 15 ps that can be traced back to originate from the $2^1\Pi_g$ surface. A contribution

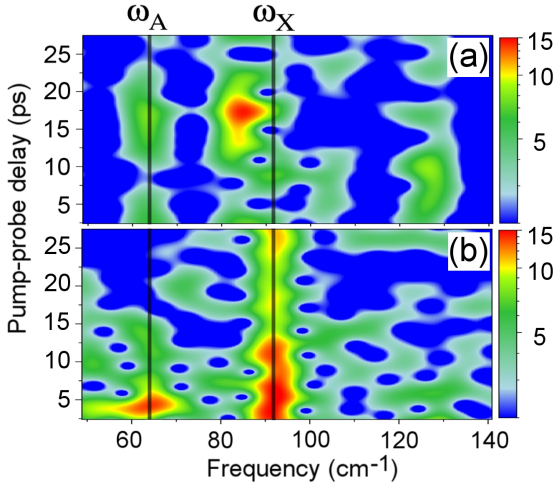

Figure 3. Spectra $\mathcal{F}(\omega, \tau)$ in the time-frequency domain at $\lambda = 800\,\mathrm{nm}$. (a) Numerical gas phase calculation, where electronic interferences lead to a spectrum that is difficult to interpret. (b) Experimental HENDI result (from [1]). Electronic interferences are absent, allowing for a clear identification of the structures of the spectrum.

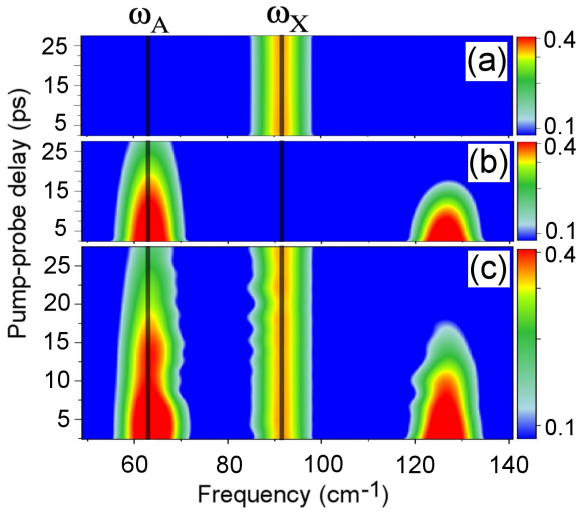

Figure 4. Shown is a the spectrogram $\mathcal{F}^i(\omega,\tau)$, which is obtained upon projecting the created full wave function $\Psi(t)$ on the electronic ground state ($i=0$) and (b) first excited state ($i=1$). (c) In the incoherent sum, interferences are excluded. In particular, the ground state component is clearly resolved.

from the ground state and resulting frequency component ω_X, however, is missing. In agreement with earlier findings [38, 36], the mapping of the ground state WP is not possible at low to intermediate intensities in the gas phase. This is because, as explained below, contributions from different potential energy surfaces interfere destructively. In contrast, for dimers attached to He droplets, the contribution from the state $\mathrm{A}\,^1\Sigma_u^+$ is suppressed after about 8 ps, while on the other hand the vibrational ground state WP is clearly resolved, see fig. 3(b).

Qualitatively, the difference between fig. 3(a) (gas phase) and fig. 3(b) (experiment) can be explained by the loss of electronic coherence alone: In fig. 4, we construct an artificial signal from the incoherent sum of contributions. The full coherent wave vector after decay of the pump pulse at $t \equiv t_{\mathrm{pump}}$, eq. (1), serves as a starting point. In order to determine the contribution of a single WP ψ_i, we project the fully coherent wave vector according to $\tilde{\Psi}_i(t_{\mathrm{pump}}) = P_i|\Psi(t_{\mathrm{pump}})\rangle$ with the projector $P_i = |i\rangle\langle i|$ on one of the electronic states. The electronic occupation p_i is not altered and the usual probe scheme is employed after projection. The resulting spectrogram $\mathcal{F}^i(\omega,\tau)$ after projection on the state $\mathrm{A}\,^1\Sigma_u^+$ and $\mathrm{X}\,^1\Sigma_g^+$, respectively, is shown in fig. 4(a)/(b). The incoherent sum of contributions is given by

$$\mathcal{F}^{\mathrm{inc}}(\omega,\tau) = \sum_i \mathcal{F}^i(\omega,\tau). \tag{6}$$

Contrary to the coherent signal, fig. 3(a), in eq. (6) interferences are removed by hand and contributions from ground- and excited state WPs are clearly visible. Obviously, the incoherent sum fig. 4(c) already reproduces important features of the experimental data. In the experiment (fig. 3(b)), however, the component ω_A fades out at later delay times, while the component ω_X becomes dominant. Therefore, a model based on pure

loss of electronic coherence alone cannot explain the measured spectrum. One has to consider additional influences of the He environment on the dimer dynamics.

3. He influence and results

In a phenomenological approach, we take into account three possible effects:

(i) A He-induced energetic shift of electronic potential energy surfaces, with possibly small fluctuations.

(ii) Damping of vibrational wave packets. This effect is treated fully quantum mechanically within the master equation approach. The WP ψ_i dissipates energy with a certain damping rate γ_i. This rate is here seen as a fit parameter and is adjusted to experimental observations.

(iii) Desorption of dimers off the droplet. After desorption, the influence of the helium droplet (shift/damping) vanishes.

A description based on damping of vibrational wave packets has been applied to HENDI studies with spin triplet Rb_2 dimers [15]. There, slow vibrational decoherence (as a consequence of very weak dissipation) is most relevant for the decay of the revival amplitude. In particular, as witnessed by the ongoing decay, desorption of dimers seems to be inhibited.

In the following, step by step, we include shift, damping and finally desorption in the calculation of pump-probe spectra. It is found that all model "ingredients" 1. - 3. are crucial to find agreement with obtained experimental spectra.

3.1. Electronic shifts

The He environment may lead to shifts of electronic surfaces in attached dimers. Such shifts are common for alkali atoms and molecules on He droplets [27]. Spectra from attached species are shifted relative to what one expects from gas-phase potential energy curves [52, 53, 54, 55, 56]. For certain weakly coupled species, spectra are only shifted by a few wavenumbers [27]. Denoting the shift of surface i with Δ_i, the full state vector is propagated according to

$$|\dot{\Psi}(t)\rangle = -\frac{i}{\hbar}H|\Psi(t)\rangle + \frac{i}{\hbar}\sum_i \Delta_i|\psi_i\rangle \tag{7}$$

Both surfaces $A\,^1\Sigma_u^+$ and $2^1\Pi_g$ may be affected. Only relative shifts are relevant for the signal, such that we cannot differentiate between a shift of the electronic ground - or first excited state. Also, a shift of the ionic surface would change the energy distribution of the ejected electrons, but not the overall calculated ion yield. This is because we sum over all electronic energies in eq. (4). We find that even large, but fixed shifts of up to $\pm 100\,\mathrm{cm}^{-1}$ have a very small influence and resemble the gas phase calculation.

However, it is reasonable to assume that the shifts Δ_i fluctuate for the following reason: The number of He atoms of a droplet is not fixed but varies according to a

log-normal distribution [57]. Consequently, we have to average over a distribution of shifts Δ_i [58]. Also, for the considered laser intensities, electronic surfaces are slightly Stark-shifted. Depending on their position in the laser beam, dimers are exposed to a distribution of laser intensities [59]. The beam width leads to a distribution of Stark shifts, which in turn has to be treated as random distribution of electronic shifts Δ_i.

Considering fluctuating potential energies, eq. (7) represents only a single realization $|\Psi_j(t)\rangle$ with shifts $\Delta_i(j)$ in the ensemble. The pump-probe signal is proportional to the ensemble average

$$\langle S(\tau)\rangle = \frac{1}{N}\sum_j \left[\lim_{t\to\infty}\sum_{E_k} |\psi_{j,3}(\tau, E_k)|^2\right], \tag{8}$$

where N realizations have been taken into account. In this expression, the final state $|\psi_{j,3}\rangle$ is obtained from propagation of the realization $|\Psi_j(t)\rangle$, in which $\Delta_i(j)$ is chosen randomly. Through the ensemble average in eq. (8), one obtains an incoherent mixture of electronic contributions in the final state. The spectrogram of $\langle S(\tau)\rangle$ nearly perfectly resembles the incoherent sum of contributions, see eq. (6) and fig. 4(c). It does not contain any electronic coherence, such that the frequency components ω_i are clearly resolved. For full decoherence fig. 4(c), random shifts in the range of $\pm 5\,\mathrm{cm}^{-1}$ around the average shifts $\overline{\Delta_1} = 0\,\mathrm{cm}^{-1}$ and $\overline{\Delta_2} = -50\,\mathrm{cm}^{-1}$ are sufficient. Note that this decoherence is due to the inhomogeneous size distribution and not due to entanglement between system and environment [60, 61].

To conclude, randomly distributed energy shifts can explain the visibility of the ground state component ω_X. However, this effect lacks an explanation for the decay of the frequency component ω_A of the excited state, which is observed in the HENDI experiment. Therefore, we consider vibrational damping next.

3.2. Damped vibrational wave packets

Dissipation can be treated fully quantum mechanically by using approximate master equations for the density operator of the (reduced) system. The overall dissipation of an excited WP originates in our case from the interaction of vibrational degrees of freedom of the molecule with collective degrees of freedom of the helium droplet. Note that in recent studies [29] vibrational relaxation rates for alkali dimers on ^{4}He clusters are estimated from full quantum Monte Carlo calculations for a few He atoms. These rates turn out to be roughly of the same order of magnitude as our phenomenologically chosen damping rates below.

In our approach, the density ρ of the damped WP in an electronic state $|i\rangle$ evolves according to the master equation

$$\dot{\rho} = -\frac{i}{\hbar}[H_i, \rho] + \gamma\left(a\rho a^\dagger - \frac{1}{2}a^\dagger a\rho - \frac{1}{2}\rho a^\dagger a\right), \tag{9}$$

which is of Lindblad form [62]. It describes friction for near-harmonic systems at effectively zero temperature in the rotating wave approximation (see, for instance,

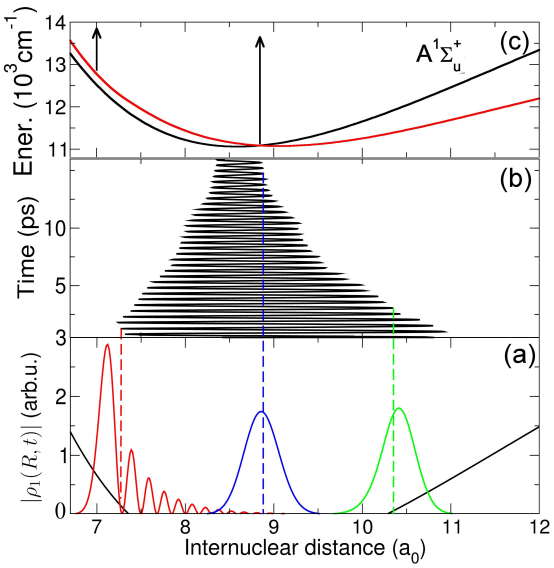

Figure 5. (a) Shown is single realization of a wave function in position space. The WP circulates in the A state and is damped with a rate $\gamma_1 = 0.3$/ps. (b) Coordinate expectation value for that single realization. The noise is due to the stochastic propagation. (c) Potential curves A (black) and 2Π (red). The latter is shifted by one photon energy ($\lambda = 800$ nm) to clarify possible transitions to the ionic state (arrows). A fully damped WP can be mapped to the final state.

[63]). The first term in eq. (9) contains the molecular Hamiltonian H_i of a specific electronic state $|i\rangle$ and determines the unitary evolution of the WP $|\psi_i\rangle$. Relaxation of the vibrational WP is achieved through the second, irreversible contribution. Any initial state approaches the ground state on a time scale γ^{-1}, i. e. γ denotes the damping rate. In eq. (9), $a, a^\dagger$ are the creation/annihilation operators of a harmonic oscillator, defined through

$$a = \frac{1}{\sqrt{2}} \left(\sqrt{\frac{\hbar}{m\omega_e}} \hat{X} + i \frac{1}{\sqrt{\hbar m \omega_e}} \hat{P} \right) . \tag{10}$$

Here, $\hat{X}$ and $\hat{P}$ are the usual position and momentum operator w.r.t. the harmonic oscillator minimum and ω_e its frequency. The quantum optical master equation (9) can be derived from a von-Neumann equation for the full system and is valid only for weak couplings between system and "bath" (which is the helium droplet here). Also, in the derivation one makes use of the Markov and rotating wave approximation. For a significant temperature, additional terms that describe thermal excitations from the environment have to be taken into account [64]. The damping constant γ may in principle be derived from a microscopic description of interaction between system and bath (Fermi's Golden Rule). We do not specify this interaction, but use the damping rate γ as a fit parameter to obtain agreement with experimental data. The master equation (9) induces the evolution of a pure initial state into a state mixture.

For the numerical propagation, we return from the density matrix description to a

Schrödinger-type equation for the state vector. It is not possible to evolve a pure state into a mixed state with a deterministic Schrödinger equation. One therefore considers a stochastic differential equation for a state vector, quantum state diffusion (QSD) [65]. The density is recovered from the average over several realizations of state vectors. Given a master equation in "Lindblad form", as in our case, it is straightforward to state the corresponding quantum state diffusion (QSD) Ito stochastic Schrödinger equation for a state vector [65]:

$$\begin{aligned} |d\psi(t)\rangle = & -\frac{i}{\hbar}H_i|\psi\rangle dt \\ & + \frac{1}{2}\gamma\left(2\langle a^\dagger\rangle a - a^\dagger a - |\langle a\rangle|^2\right)|\psi\rangle dt + \sqrt{\gamma}(a-\langle a\rangle)|\psi\rangle d\xi(t). \end{aligned} \tag{11}$$

The left hand side means $|d\psi(t)\rangle = |\psi(t+dt)\rangle - |\psi(t)\rangle$, i. e. the change of the state after a time increment dt. The second term induces transitions to lower lying vibrational states. The third term is stochastic and contains complex normalized Ito increments $d\xi(t)$, which satisfy

$$\begin{aligned} d\xi^2 &= (d\xi^*)^2 = 0 \\ d\xi d\xi^* &= dt. \end{aligned} \tag{12}$$

The increment of the density up to second order in dt is given through $d\rho = |d\psi\rangle\langle\psi| + |\psi\rangle\langle d\psi| + |d\psi\rangle\langle d\psi|$. Since eq. (11) is written in Ito form, one can easily take the average with respect to (12) and prove the equivalence with the given master equation (9). Recovering the density $\rho = \overline{|\psi(t)\rangle\langle\psi(t)|}$ from several realizations of $|\psi\rangle$ amounts to obtaining expectation values through $\langle A\rangle = \mathrm{Tr}(A\rho) = \overline{\langle\psi|A|\psi\rangle}$. In fig. 5 we show the coordinate expectation value $\langle R\rangle$, obtained from a single realization of $|\psi\rangle$. The norm of the state in eq. (11) is conserved, i. e. $d(\langle\psi|\psi\rangle) = 0$. However, due to the finite time step Δt, the norm can slightly fluctuate. Therefore, for the numerics, we impose norm preservation by renormalizing the state vector after every time step. After replacing the ladder operators in eq. (11) through their definition in (10), the r. h. s. is strictly separable in operators, which act in either momentum or coordinate space. Therefore, the split operator method [49] for the propagation of the WP can still be used, which is an advantage of this approach.

Helium induced damping of vibrational wave packets on a *single* electronic surface is described through eq. (11), which is equivalent to the master equation eq. (9) on average. In order to obtain damping on several electronic surfaces, we propagate a full state vector $|\Psi(t)\rangle$ according to

$$|d\Psi(t)\rangle = -\frac{i}{\hbar}H|\Psi(t)\rangle dt + \underbrace{\sum_j \left[D(\gamma_j) + \frac{i}{\hbar}\Delta_j\right]|\psi_j\rangle}_{\text{coupling to He bath}} \tag{13}$$

The average is taken over several realizations of state vectors to recover the density via $\rho(t) = \overline{|\Psi(t)\rangle\langle\Psi(t)|}$. In eq. (13), $D(\gamma_j)$ is the generalization of the r.h.s. of eq. (11) to obtain damping and accompanying fluctuations on an arbitrary surface,

$$D(\gamma_j) = \frac{1}{2}\gamma_j\left(2\langle a_j^\dagger\rangle a_j - a_j^\dagger a_j - |\langle a_j\rangle|^2\right)dt + \sqrt{\gamma_j}(a_j - \langle a_j\rangle)d\xi_j(t) \tag{14}$$

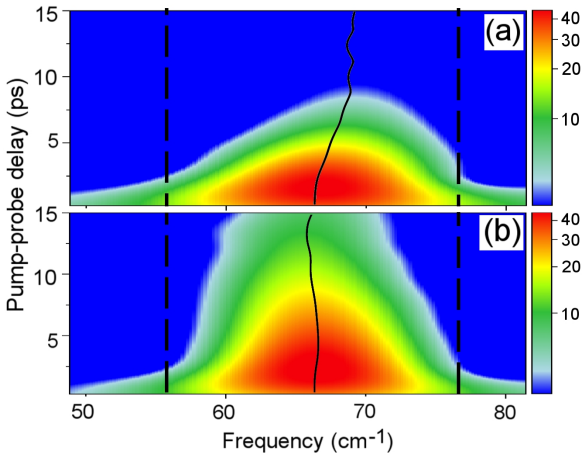

Figure 6. Spectra $\mathcal{F}(\omega, \tau)$ in the time-frequency domain at $\lambda = 833\,\text{nm}$. (a) Full damping. (b) Damping and state-dependent desorption. Also shown is the frequency upon averaging in the lined frequency interval. Explanation see text.

In eq. (14), all stochastic differential Wiener increments $d\xi_j$ are taken independently of each other. In the ladder operator of surface j, one uses the the position w.r.t. the respective harmonic oscillator minimum and its frequency. For most parts of the following, for simplicity, we set damping constants to be equal $\gamma_j = \gamma$. However, we hasten to add that an interesting exception is provided in section 3.4. The agreement with experiment improves, if one allows for *undamped* vibrational motion in the electronic ground state, $\gamma_0 = 0$.

The damping model provides an explanation for the signal decrease at $\lambda = 833\,\text{nm}$ (excitation scheme I). After several periods, vibrationally damped WPs on the A surface no longer enter the initial FC region and therefore the ion yield decreases. In fig. 6 we depict the result of the damping model eq. (13), using $\gamma_1 = 0.15/\text{ps}$. Clearly visible is a shift of the central frequency $\omega_A \to \omega'_A > \omega_A$, since the WP relaxes to lower vibrational levels. A frequency shift is also observed experimentally [1]. In the full damping model, however, the signal decays to zero, since at this wavelength vibrational relaxation leads to a complete "closing" of the initial FC window. This result is in contrast to the experimental observation, where a pronounced oscillation is also present at later delay times, see [1] and fig. 2(b), and requires further studies below.

At $\lambda = 800\,\text{nm}$ (excitation scheme II), full damping leads to the result shown in fig. 7(a). Through dissipation, the WP in the state $A\,^1\Sigma_u^+$ leaves the initial FC region. However, the decelerated WP approaches another FC window around the equilibrium distance, cf. fig. 5, after several circulations. The signal therefore shows a massive increase of the (shifted) frequency component ω'_A.

For both excitation schemes, the inclusion of damping improves agreement with experiment for the first $\simeq 10\,\text{ps}$. However, at later times, there are still significant discrepancies. These can be removed by taking into account desorption of dimers off the droplet.

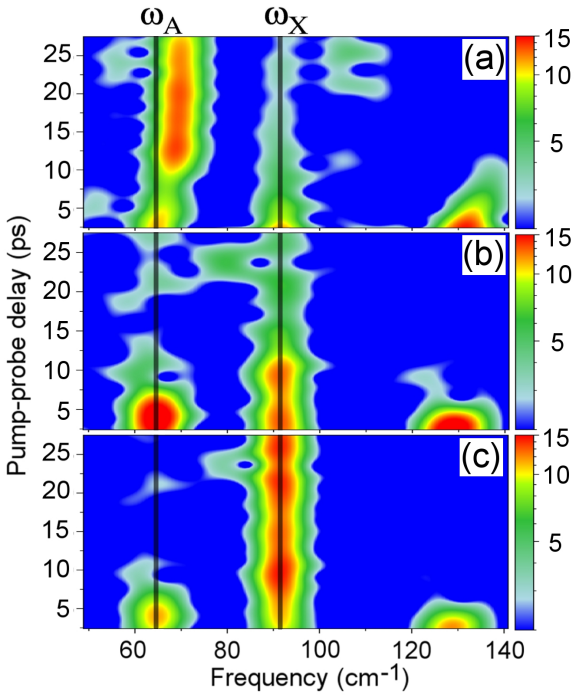

Figure 7. Calculated spectra in the time-frequency domain at $\lambda = 800\,\mathrm{nm}$. (a) Full damping: The WP in the A state leaves the initial transition region, consequently the component ω_A decreases. The fully damped WP, however, reaches a transition region at the equilibrium distance, such that ω_A returns. See also fig. 5. (b) State-dependent desorption model. (c) State-dependent desorption model together with undamped motion in the ground state.

The clear visibility of both frequency components ω'_A and ω_X is again attributed to electronic decoherence: Since the damping scheme is carried out (stochastically) independent on all involved electronic states, damping leads to electronic decoherence similar to the fluctuating shifts we assumed previously. The final signal is an incoherent mixture of electronic contributions, as previously considered through eq. (6). However, a massive increase of the component ω'_A is not observed experimentally (compare fig. 3(b) and fig. 7(a)).

Desorption of the dimer off the droplet prevents the full vibrational damping in the electronic ground or excited state. Indeed, as we will show, desorption implies the disappearance of component ω_A and simultaneous ongoing presence of ω_X. For excitation scheme I, desorption explains the observed signal oscillation at later delay times.

3.3. Desorption

The release of a dimer into the gas phase takes place at some random time t'. In our model, a state vector evolves according to eq. (13) up to time t'. As the He influence vanishes at t', shift/damping terms in eq. (13) are set to zero. We have to consider

the ion yield at delay time τ, which is changed because of the dissapearance of the He influence at time t'. If the desorption occurs before the decay of the probe pulse ($t' \lesssim \tau$), the resulting signal is denoted as $S(\tau, t')$. If the desorption occurs after decay of the probe pulse ($t' \gtrsim \tau$), the ion yield is unaffected by the desorption process. Anything that happens after the probe pulse, will not be mapped to the ion yield. The resulting signal is denoted with $S(\tau, \tau)$.

Note that in an ensemble of attached dimers, the desorption time t' will be distributed according to some probability distribution $P(t')$. We therefore have to calculate the pump-probe signal for various desorption times t' and consider the averaged signal.

We first assume that the electronic state occupation is not relevant in the desorption process. A dimer therefore has a certain probability to stay on or leave (still being in the superposition) the droplet, but this probability is independent of the specific electronic occupation. We assume a constant probability

$$p_{\text{off}}(t', t' + \Delta t') = \Delta t' R_D \tag{15}$$

that the dimer leaves the droplet within a small time interval $(t', t' + \Delta t)$. Here, R_D marks the constant desorption rate. The probability to find the dimer attached at arbitrary time t' is hence given through

$$P_{\text{on}}(t') = e^{-t' R_D}. \tag{16}$$

The signal contains weighted contributions and is obtained from

$$\begin{aligned} \langle S(\tau) \rangle &= R_D \int_0^\infty P_{\text{on}}(t') S(\tau, t') dt' \\ &= P_{\text{on}}(\tau) S(\tau, \tau) + R_D \int_0^\tau P_{\text{on}}(t') S(\tau, t') dt'. \end{aligned} \tag{17}$$

In the second line we have used that for $t' \gtrsim \tau$ (desorption after decay of the probe pulse) the ion yield does not change. In this case, the dimer is fully damped until the probe pulse has passed.

In a previous study, we made use of the state-independent desorption scheme eq. (17), see Ref. [2]. Although it is possible to find reasonable agreement with experimental findings, it is an oversimplification to not take into account the electronic state for desorption. It is likely that only electronically excited dimers leave the droplet. The electronic excitation implies a larger degree of distortion of the helium enviroment [44]. On the other hand, it is reasonable to assume that (slowly moving) ground state systems stay attached. Therefore, we consider an alternative desorption scheme and only allow excited dimers to leave the droplet. Desorption is again described in terms of a constant in time desorption rate R_D. The probability for the molecule to desorb, however, is now proportional to the excitation probability $p_{\text{e}} = \sum_{i \neq 0} p_i$, such that eq. (15) is replaced by

$$p_{\text{off}}(t', t' + \Delta t') = p_{\text{e}} R_D \Delta t'. \tag{18}$$

Note that in this scheme, the state after desorption does not contain any electronic ground state component (see later). Those dimers that do not desorb evolve according to the dissipative dynamics eq. (13). In order to compensate for apparent loss of ground state dimers, we need a third possible channel: With probability $p_{\mathrm{g}} R_D \Delta t' = (1 - p_{\mathrm{e}}) R_D \Delta t'$ the dimer remains on the droplet and is projected onto its electronic ground state. For the full averaged signal, we obtain

$$\langle S_{\mathrm{SD}}(\tau) \rangle = P_{\mathrm{on}}(\tau) S(\tau, \tau) + p_{\mathrm{e}} R_D \int_0^\tau P_{\mathrm{on}}(t') S_{\mathrm{e}}(\tau, t') dt' + p_{\mathrm{g}} R_D \int_0^\tau P_{\mathrm{on}}(t') S_{\mathrm{g}}(\tau, t') dt'. \tag{19}$$

$S_{\mathrm{e}}(\tau, t')$ is the signal obtained upon removal of the helium influence at time $t' \lesssim \tau$ and subsequent projection on the excited superposition of electronic state. Likewise, $S_{\mathrm{g}}(\tau, t')$ is obtained upon projection on the ground state. Note that a renormalization of the full wavefunction $|\Psi\rangle$ is required after projection, such that $\sum p_i = 1$ is always valid.

In fig. 6(b), we show the spectrogram for $\langle S_{SD}(\tau) \rangle$ at $\lambda = 833\,\mathrm{nm}$ (scheme I). We use a desorption rate $R_D = 0.1/\,\mathrm{ps}$, while the damping/shift parameters are not changed (as before , $\gamma = 0.15/\mathrm{ps}$ and $\Delta_2 = -50\mathrm{cm}^{-1}$). In the spectrogram, a (small) frequency shift is $\omega_A \to \omega'_A$ is observable. The shift is mainly due to contributions of vibrationally damped dimers by means of the first term in eq. (19). We obtain a frequency shift $\omega_A \to \omega'_A$ in the model, but the shift is more pronounced in the experiment [1]. The second term in eq. (17) marks contributions from dimers which are damped up to time $t' \lesssim \tau$, but are not damped afterwards, i. e. upon release from the droplet. Early desorbing dimers are not vibrationally relaxed and the WP in the $\mathrm{A}\,^1\Sigma_u^+$ state continous to reach the initial FC region. From this point of view, undamped dimers may well contribute to the ion yield. Indeed, contributions to the ion yield at later delay times $t \gtrsim 20\,\mathrm{ps}$ are exclusively attributed to these undamped dimers. There, the oscillation frequency is near the initial gas phase value $\omega_A = \omega_{\bar{v},\bar{v}+1}$.

As a final note, we find that the observed frequency shift $\omega_A \to \omega'_A$ becomes negligible if we do not include the electronic shift Δ_2 in the model.

As the laser frequency is further increased, the vibrational energy of the WP in the $\mathrm{A}\,^1\Sigma_u^+$ state increases (scheme II). Due to the larger elongation and faster dynamics, one may think of larger damping of vibrational motion and/or faster desorption of dimers off the droplet. In fig. 7(b) we show the spectrogram at $\lambda = 800\,\mathrm{nm}$, as obtained for $\gamma_i = 0.15/\mathrm{ps}$ and $R_D = 0.5/\mathrm{ps}$, i. e. we assume a faster desorption as before for scheme I. In fact, this value for the desorption rate means that dimers quickly leave the droplet after the pulse excitation. Until desorption, electronically excited dimers are fully damped. During that time, they approach an intermediate transition region with smaller overlap with higher electronic states, see fig. 5(c). As a consequence, the component ω_A fades away after several picoseconds. Also, vibrational WPs of desorbed dimers do not reach the FC window at the equilibrium distance, which is also marked in fig. 5(c). Therefore, an increase of the component ω_A is excluded, compare fig. 7(a) and (b). To conclude, damping in connection with fast desorption of dimers explains

the experimental result, see fig. 3(b), where the component ω_A is only visible in the beginning of the measurement and then disappears. Note that dimers which remain on the droplet in the ground state, are fully damped. Therefore, the ground state component ω_X decreases in this model.

3.4. Undamped ground state WPs

Agreement with experiment can be further improved, if one allows for undamped motion of the vibrational WP in the ground state. This is of particular relevance for excitation scheme II, for which the result upon leaving the model parameters for damping, desorption and shift unchanged, but setting $\gamma_0 = 0$, is shown in fig. 7(c). Frequency components at later delay times are exclusively attributed to the ground state motion, i. e. the component ω_X is clearly visible. Undamped vibrational wave packet motion has been discussed in terms of a critical Landau velocity v_{crit} in Ref.[2]. The existence of v_{crit} in the superfluid nanodroplet may allow for frictionless motion of slowly moving ground state WPs. In fig. 7(c) the ground state motion is assumed frictionless; good agreement with the experimental result, see fig. 3(b), is also obtained for nearly frictionless motion $\gamma_0 \approx 0$.

Note that for the observation of the ground state WP, the electronic shift Δ_2 is less important. It only leads to a slightly different ratio between the ground-and excited state frequency component.

4. Conclusions

We consider vibrational wave packet dynamics of dimers attached to He nanodroplets. It is found that (calculated) gas phase spectra and spectra from dimers attached to He droplets are markedly different. The interaction between droplet and dimer influences the vibrational dimer dynamics in three ways: Shifts, damping, and desorption. All three ingredients are taken into account in a phenomenological manner and each contributes to characteristic changes of the resulting spectra.

First, we study electronic decoherence, occurring for instance due to slightly fluctuating shifts of electronic surfaces. We find that, indeed, resulting spectra do not show electronic interferences such that contributions from several electronic states, in particular the ground state, are clearly resolved. In this way, the modeled spectrum is already similar to the experimental finding.

However, pure electronic decoherence cannot explain a decreasing contribution to the signal from wave packets in the first excited $A\,^1\Sigma_u^+$ state. Consequently, vibrational damping of wave packets is taken into account, which improves agreement with experiment for short delay times. We find that damping is not present over the full observation timescale, probably due to desorption of dimers from the droplet. We use a desorption scheme, which takes into account the occupation of electronic levels. We find that the desorption rate depends on the mean vibrational energy of the wave

packet. At $\lambda = 800\,\mathrm{nm}$, desorption is fast, taking place on average several picosecond after excitation ($R_D = 0.5/\mathrm{ps}$).

Note that in this study, all involved electronic states are spin singlet states. For the WP in these singlet states, we find a relaxation rate which is significantly higher than in previously considered spin triplet Rb_2 dimers attached to He droplets. The smaller rate in the latter may be ascribed to the orientation of the dialkali axis relative to the droplet surface. Recent calculations show that the axis of spin triplet dimers is oriented parallel to the droplet surface while singlet states are assumed to be oriented perpendicularly [66, 29]. Upon the perpendicular orientation in our case, the dimer might interact with the droplet more efficiently, such that relaxation is faster.

Damping appears to be absent for (slowly moving) wave packets in the electronic ground state. There, vibrational motion is found to be nearly frictionless. A potential energy surface for the dimer-droplet system, which is currently underway for Rb_2 [66], should give additional insight on dissipation rates of the wave packet.

The authors would like to thank Marcel Mudrich and Frank Stienkemeier for providing experimental data, for fruitful discussions and helpful comments. Further, we thank Alexander Eisfeld for valuable remarks. Support by the Deutsche Forschungsgemeinschaft through the research grant "Control and Coherence of the Few-Particle Continuum" is gratefully acknowledged. Computing resources have been provided by the Zentrum für Informationsdienste und Hochleistungsrechnen (ZIH) at the TU Dresden. M. S. is a member of the IMPRS Dresden.

[1] Claas P, Droppelmann G, Schulz C P, Mudrich M and Stienkemeier F 2006 *J. Phys. B* **39** S1151
[2] Schlesinger M, Mudrich M, Stienkemeier F and Strunz W T 2010 *Chem. Phys. Lett.* **490** 245–248
[3] Toennies J P and Vilesov A F 2004 *Angew. Chem., Int. Ed.* **43** 2622–2648
[4] Stienkemeier F and Lehmann K K 2006 *J. Phys. B* **39** R127
[5] Callegari C, Reinhard I, Lehmann K K, Scoles G, Nauta K and Miller R E 2000 *J. Chem. Phys.* **113** 4636–4646
[6] Lehmann K K 1999 *Mol. Phys.* **97** 645–666
[7] Callegari C, Lehmann K K, Schmied R and Scoles G 2001 *J. Chem. Phys.* **115** 10090–10110
[8] Reho J, Callegari C, Higgins J, Ernst W E, Lehmann K K and Scoles G 1997 *Faraday Discussions* **108** 161–174
[9] Grebenev S, Toennies J P and Vilesov A F 1998 *Science* **279** 2083–2085
[10] Callegari C, Conjusteau A, Reinhard I, Lehmann K K and Scoles G 1999 *Phys. Rev. Lett.* **83** 5058–5061
[11] Nauta K and Miller R E 2001 *J. Chem. Phys.* **115** 45084514
[12] Dick B and Slenczka A 2001 *J. Chem. Phys.* **115** 10206–10213
[13] Hartmann M, Mielke F, Toennies J P and Vilesov A F 1996 *Phys. Rev. Lett.* **76** 4560–4563
[14] Mudrich M, Heister P, Hippler T, Giese C, Dulieu O and Stienkemeier F 2009 *Phys. Rev. A* **80** 042512
[15] Grüner B, Schlesinger M, Heister P, Strunz W T, Stienkemeier F and Mudrich M 2011 *Phys. Chem. Chem. Phys.* **13** 6816–6826 ISSN 1463-9076 URL `http://dx.doi.org/10.1039/C0CP02355H`
[16] Koch M, Auböck G, Callegari C and Ernst W E 2008 *Phys. Rev. Lett.* **103** 035302
[17] Braun A and Drabbels M 2004 *Phys. Rev. Lett.* **93** 253401
[18] Przystawik A, Göde S, Döppner T, Tiggesbäumker J and Meiwes-Broer K H 2008 *Phys. Rev. A* **78** 021202
[19] Kornilov O, Wang C C, Bünermann O, Healy A T, Leonard M, Peng C, Leone S R, Neumark D M and Gessner O 2010 *J. Chem. Phys. A* **114** 1437

[20] Droppelmann G, Bünermann O, Schulz C P and Stienkemeier F 2004 *Phys. Rev. Lett.* **93** 0233402
[21] Nitzan A, Mukamel S and Jortner J 1975 *J. Chem. Phys.* **63** 200
[22] Ewing G E 1987 *J. Phys. Chem. A* **91** 4662–4671
[23] Nauta K and Miller R E 2000 *J. Chem. Phys.* **113** 9466–9469
[24] Dalfovo F 1994 *Z. Phys. D* **29** 61–66
[25] Ancilotto F, DeToffol G and Toigo F 1995 *Phys. Rev. B* **52** 16125–16129
[26] Stienkemeier F, Higgins J, Ernst W E and Scoles G 1995 *Phys. Rev. Lett.* **74** 3592–3595
[27] Higgins J, Callegari C, Reho J, Stienkemeier F, Ernst W E, Gutowski M and Scoles G 1998 *J. Phys. Chem. A* **102** 4952–4965
[28] Bovino S, Bodo E, Yurtsever E and Gianturco F A 2008 *J. Chem. Phys.* **128** 224312
[29] Bovino S, Coccia E, Bodo E, Lopez-Duran D and Gianturco F A 2009 *J. Chem. Phys.* **130** 224903
[30] Zewail A H 1993 *J. Phys. Chem.* **97** 12427
[31] Gruebele M, Roberts G, Dantus M, Bowman R M and Zewail A H 1990 *Chem. Phys. Lett.* **166** 459–469
[32] Baumert T, Engel V, Röttgermann C, Strunz W T and Gerber G 1992 *Chem. Phys. Lett.* **191** 639–644
[33] Bowman R, Dantus M and Zewail A 1989 *Chem. Phys. Lett.* **161** 297
[34] Gruebele M and Zewail A H 1993 *J. Chem. Phys.* **98** 883
[35] Baumert T, Bühler B, Grosser M, Weiss V and Gerber G 1991 *J. Phys. Chem.* **8103** 8103–8110
[36] de Vivie-Riedle R, Kobe K, Manz J, Meyer W, Reischl B, Rutz S, Schreiber E and Wöste L 1996 *J. Phys. Chem.* **100** 7789–7796
[37] Rutz S and Schreiber E 1997 *Chem. Phys. Lett.* **269** 9
[38] Nicole C, Bouchène M A, Meier C, Magnier S, Schreiber E and Girard B 1999 *J. Chem. Phys.* **111** 7857
[39] Karavitis M, Segale D, Bihary Z, Pettersson M and Apkarian V A 2003 *Low Temp. Phys.* **29** 814
[40] Gühr M, Ibrahim H and Schwentner N 2004 *Phys. Chem. Chem. Phys.* **6** 5353–5361
[41] Meier C 2004 *Phys. Rev. Lett.* **93(17)** 173003(4)
[42] Liu Q, Wan C and Zewail A H 1996 *J. Phys. Chem. A* **100** 18666
[43] Schlesinger M and Strunz W T 2008 *Phys. Rev. A* **77** 012111
[44] Stienkemeier F and Vilesov A F 2001 *J. Chem. Phys.* **115** 10119–10137
[45] Reho J, Callegari C, Higgins J, Ernst W E, Lehmann K K and Scoles G 1997 *Faraday Discuss.* **108** 161–174
[46] Schulz C P, Claas P and Stienkemeier F 2001 *Phys. Rev. Lett.* **87** 153401
[47] Auböck G, Nagl J, Callegari C and Ernst W E 2008 *Phys. Rev. Lett.* **101** 035301
[48] de Vivie-Riedle R, Reischl B, Rutz S and Schreiber E 1995 *J. Phys. Chem.* **99** 16829–16834
[49] Feit M, Fleck F and Steiger A 1982 *J. Comp. Phys.* **47** 412–433
[50] Fischer I, Vrakking M J J, Villeneuve D M and Stolow A 1996 *Chem. Phys.* **207** 331–354
[51] Vrakking M J J, Villeneuve D M and Stolow A 1996 *Phys. Rev. A* **54** R37
[52] Stienkemeier F, Higgins J, Callegari C, Kanorsky S I, Ernst W E and Scoles G 1996 *Zeitschrift Fur Physik D-Atoms Molecules And Clusters* **38** 253–263
[53] Allard O, Nagl J, Aubock G, Callegari C and Ernst W E 2006 *J. Phys. B* **39** S1169–S1181
[54] Brühl F R, Miron R A and Ernst W E 2001 *J. Chem. Phys.* **115** 10275–10281
[55] Auböck G, Aymar M, Dulieu O and Ernst W E 2010 *J. Chem. Phys.* **132** 054304
[56] Bünermann O, Droppelmann G, Hernando A, Mayol R and Stienkemeier F 2007 *J. Phys. Chem. A* **111** 12684
[57] Lewerenz M, Schilling B and Toennies J P 1993 *Chem. Phys. Lett.* **206** 381–387
[58] Loginov E 2008 *Photoexcitation and photoionization dynamics of doped liquid helium-4 nanodroplets* Ph.D. thesis Lausanne : EPFL
[59] Mudrich M private communication
[60] Schlosshauer M 2007 *Decoherence And The Qantum-To-Classical Transition* (Berlin: Springer)
[61] Helm J and Strunz W T 2009 *Phys. Rev. A* **80** 042108

[62] Lindblad G 1975 *Commun. Math. Phys.* **40** 147–151
[63] Scully M O and Zubairy M S 1997 *Quantum Optics* (Cambridge: Cambridge University Press)
[64] Breuer H and Petruccione F 2002 *The theory of open quantum systems* (Oxford: Oxford University Press)
[65] Gisin N and Percival I C 1992 *J. Phys. A: Math. Gen.* **25** 5677–5691
[66] Guillon G, Zanchet A, Leino M, Viel A and Zillich R E 2011 *J. Phys. Chem. A* **115** 6918–6926